Materials Today Bio 23 (2023) 100822

Contents lists available at ScienceDirect

Materials Today Bio

journal homepage: www.journals.elsevier.com/materials-today-bio

NIR-triggered photodynamic therapy of traumatic heterotopic ossification with a type II collagen-targeted photosensitizer

Zheng Wang [1], Chao Sun [1], Yifeng Yu, Dong Zhang, Baiwen Qi, Zonghuan Li [*], Xinzeyu Yi [**], Aixi Yu [***]

Department of Orthopedics Trauma and Microsurgery, Zhongnan Hospital of Wuhan University, Wuhan, 430071, China

ARTICLE INFO

Keywords:
Photodynamic therapy
ROS
Heterotopic ossification
Cartilage
Targeted therapy

ABSTRACT

Traumatic heterotopic ossification (HO) represents an intractable sequela following trauma with no currently effective prophylaxis or treatment. Photodynamic therapy (PDT) is a non-invasive treatment for various proliferative diseases. However, the specific effects of PDT on HO development remain unclear. In this study, the therapeutic potential of a near-infrared (NIR) probe-WL-808, composed of type II collagen-binding peptide (WYRGRL) and a PDT photosensitizer (IR-808), was evaluated for the innovative HO-targeted PDT approach. *In vitro* studies indicated that WL-808 could induce chondrocyte apoptosis and inhibit cell viability through ROS generation under NIR excitation. *In vivo*, the efficacy of WL-808-mediated PDT was tested on the tenotomy HO model mice. WL-808 specifically targeted the type II collagen cartilaginous template of HO, promoting cell apoptosis and enhancing extracellular matrix (ECM) degradation under 808 nm NIR excitation, which inhibited the final ectopic bone formation. Moreover, no obvious toxicity or side effects were detected after treatment with WL-808. Taken together, WL-808-mediated PDT significantly diminished ectopic cartilage and subsequent bone formation, providing a new perspective for HO prophylaxis and treatment.

1. Introduction

Traumatic heterotopic ossification (HO) is an intractable sequela that occurs after orthopedic surgeries, burns, and neurologic injuries. HO is characterized by the pathological differentiation of stromal cells of mesenchymal origin, resulting in the inappropriate deposition of the cartilage and bone matrix at extraskeletal sites, such as tendons and muscles [1]. The debilitating nature of HO is evidenced by its capacity to cause severe symptoms and complications, including chronic pain, diminished range of joint motion, impaired prosthetic wearing, neurovascular compression, and poor wound healing, all of which lead to reduced quality of life [2]. Despite surgical resection being the current standard therapeutic option for symptomatic HO, it has a high recurrence rate [3]. Limited prophylactic measures, including radiotherapy and non-steroidal anti-inflammatory drugs, may lead to severe systemic or adjacent tissue complications due to the lack of targeting ability [4,5]. Consequently, there is an urgent clinical need to develop a safe, effective and non-invasion therapy with minimal adverse reactions for HO prevention and treatment.

Although the etiology of HO remains unclear, studies research suggests that the cartilaginous intermediary plays a major role in the pathogenesis of HO, as observed in the burn/tenotomy or *ACVR1*$^{fl/wt}$ HO models [6–9]. In both cases, ectopic bone formation occurs through two steps: chondrocytes initially undergo proliferation and hypertrophy to form a template-cartilage extracellular matrix, on which osteoblasts then undergo differentiation to produce matrix calcification [10,11]. Previous studies have demonstrated that conditional deletion of vascular endothelial growth factor-A (VEGFA), a crucial pro-osteogenic cue during normal bone development and homeostasis, in chondrocytes, significantly reduces HO volume [12]. Additionally, inhibition of hypoxia inducible factor-1α (Hif1α), one particular signaling mediator critical for normal chondrogenesis [13,14], effectively suppresses HO formation in the initial step [15,16]. Therefore, targeting the early phase of HO development-cartilage formation and the chondrocytes that play a

* Corresponding author.
** Corresponding author.
*** Corresponding author.
E-mail addresses: lizonghuan@whu.edu.cn (Z. Li), yxzy_zn@whu.edu.cn (X. Yi), yuaixi@whu.edu.cn (A. Yu).
[1] These authors contributed equally to this study.

https://doi.org/10.1016/j.mtbio.2023.100822
Received 10 July 2023; Received in revised form 24 September 2023; Accepted 25 September 2023
Available online 27 September 2023

key role at this stage would be sufficient to minimize or inhibit HO formation.

Photodynamic therapy (PDT) is a non-invasive and spatiotemporally controllable modality used for various proliferative diseases like malignant carcinomas and hypertrophic scars [17–26]. The mechanism of PDT involves a photosensitizer generating high levels of reactive oxygen species (ROS) under appropriate light irradiation to induce the apoptosis of the over-proliferating tumor cells or fibroblasts. Previous study has also shown that ROS-induced oxidative stress contributes to the dysfunction and apoptosis of chondrocytes as well as the progressive degradation of extracellular matrix (ECM), which plays a crucial pathogenic role in osteoarthritis development [27–29]. Furthermore, a loss of functional chondrocytes was observed in tissue culture after 5-aminolevulinic acid-based PDT (5-ALA-PDT), with increasing light doses progressively negatively affecting the cartilage [30]. As mentioned above, HO can also be classified as a proliferative disease characterized by inappropriate deposition of the bone and cartilage matrix within extraskeletal sites. However, the specific effects of ROS generated by PDT on early cartilage formation in HO are still unknown.

In our prior work, we developed a near-infrared (NIR) probe called WL-808 for early HO diagnosing by targeting type II collagen (Col2a1) in the HO cartilage lesions, which allows detecting HO formation as early as one one-week post-surgery through NIR imaging [31]. The probe consists of a Col2a1-binding peptide (WYRGRL) and a cyanine dye (IR-808), of which IR-808 has demonstrated excellent photodynamic properties for treating tumors [32]. In this study, we first evaluated the photodynamic property of WL-808. Then, both *in vitro* and *in vivo* studies were carried out to investigate the effect of ROS generated by PDT on the inhibition of HO cartilage and bone lesion formation using 808 nm irradiation, with the assistance of WL-808 (Scheme 1).

2. Experimental section

2.1. Characterization and single oxygen detection of WL-808

The absorption and emission spectra of WL-808 and YW-808 in FBS (2.5 mM) were examined with a SpectraMaxs M2 Microplate Reader (Molecular Devices, USA). Singlet oxygen ($^1O_2$) sensor green (SOSG, MesGen Biotechnology, China) was used to detect $^1O_2$ generation. Firstly, 1 mL WL-808 or IR-808 (10 μM) and SOSG (2.5 μM) were mixed and irradiated with an 808 nm laser for 2 min (1 W/cm^2). Then, an appropriate amount of solution was placed on the SpectraMaxs M2 Microplate Reader to detect singlet oxygen generation.

2.2. Dark cytotoxicity evaluation

Chondrocytes were seeded in 96-well plates at a density of 10,000 cells/well. Then, cells were treated with different concentrations of WL-808 or IR-808 (0, 0.1, 1, 2.5, 5, 10, 20, 50 and 100 μM) for 24 h and 48 h. The culture medium was replaced by 100 μl fresh medium with 10 μl of CCK-8 solution (Biosharp, China) for 2 h. The absorption was evaluated at 450 nm using a microplate reader (Thermo Fisher Scientific, USA).

2.3. Cellular uptake and localization assay

Chondrocytes were seeded into 20-mm confocal laser dishes (NEST, China) at a density of 10,000 cells/well. The cells were then incubated with WL-808 or IR-808 (20 μM) for 30 min, 1 h, 2 h, 4 h and 6 h. Hoechst 33342 was used to stain the nuclei. The subcellular localization of WL-808 or IR-808 on the mitochondria in chondrocytes was assessed using the Mito-Tracker Green (Beyotime Biotechnology, China). After Hoechst 33342 staining, the cells were sequentially incubated with 200 nM Mito-Tracker Green for 30 min and 20 μM WL-808 or IR-808 for 2 h. The fluorescence signals were detected with a confocal laser scanning microscope (CLSM, Leica, Germany) at 430–480 nm (λex = 405 nm) for Hoechst 33342, 500–550 nm (λex = 488 nm) for Mito-Tracker Green, and 650–800 nm (λex = 638 nm) for WL-808 or IR-808.

2.4. Intracellular ROS generation assay

Chondrocytes were seeded into 24-well plates at a density of 10,000 cells/well and incubated for 24 h. Hoechst 33342 was used to stain the nuclei. Following treatment with 20 μM WL-808 or IR-808 for 2 h, the cells were incubated with 10 μM of DCFH-DA (Beyotime Biotechnology, China) for 20 min. Subsequently, DCFH-DA was removed, and the cells were treated in the dark or irradiated (808 nm; 1 W/cm^2) for 3min on ice to eliminate the photothermal effect. An 808-nm laser device (Lasever, China) was used to provide irradiation. ROS generation was detected using CLSM.

2.5. Cell apoptosis assay after PDT therapy

Chondrocytes were seeded into 6-well plates at a density of 10,000 cells/well. After 2 h of incubation with 10 μM WL-808 or IR-808, the

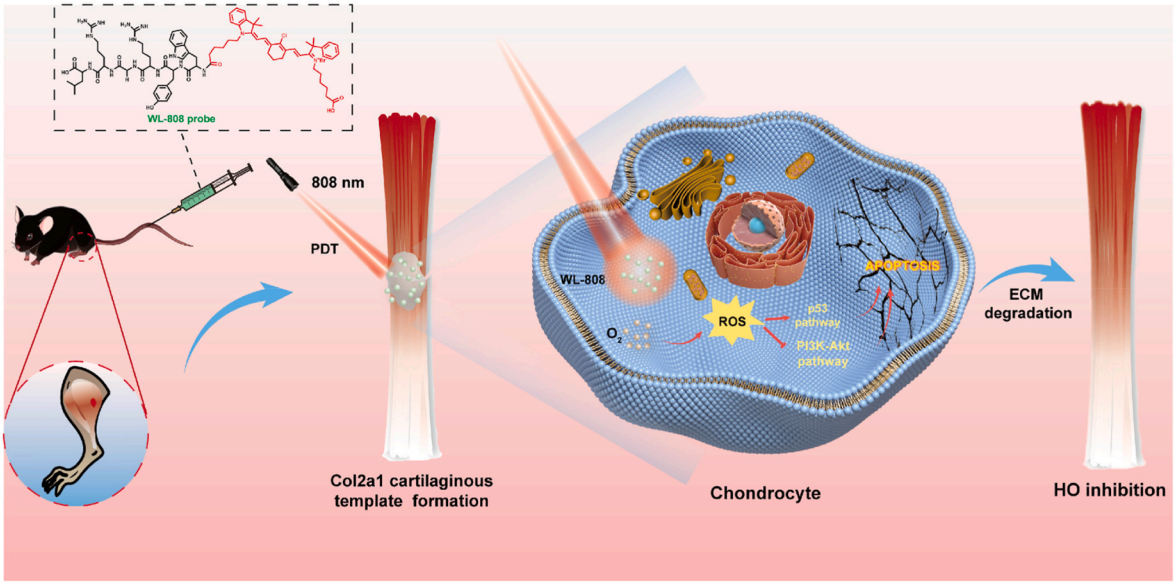

Scheme 1. Schematic illustration of WL-808 with NIR irradiation generating ROS to inhibit HO formation.

cells were irradiated (808 nm, 1 W/cm^2) for 2 min on ice. Apoptosis analysis was conducted 24 h later with the Annexin V Binding Buffer apoptosis detection kit (Elabscience, China) following the protocol. The signal was measured using a flow cytometer.

2.6. Cell viability evaluation after PDT therapy

Chondrocytes were seeded into 24-well plates at a density of 10,000 cells/well. After treatment with 20 μM WL-808 or IR-808 for 2 h, the cells were irradiated (808 nm, 1 W/cm^2) for 2min on ice. A calcein-AM/PI double stain kit (KeyGEN BioTECH, China) was used to dye dead and live chondrocytes after 24 h according to the protocol. The fluorescence signals were measured using a fluorescence microscope following the manufacturer's instructions.

2.7. Western blotting

Western blotting was performed to evaluate protein expression. Total protein was extracted using a radioimmunoprecipitation assay buffer, while nuclear protein was extracted using a nuclear protein extraction kit. Western blot analysis was performed as previously described [33]. The relevant information about all primary antibodies is listed in Table S1. The blots were visualized using enhanced chemiluminescence on an imaging system and the gel imaging software was utilized for photograph and analysis.

2.8. Establishment of the HO model

All animal experiments were performed according to the Guide for the Care and Use of Laboratory Animals of the National Institutes of Health and approved by the Experimental Animal Welfare Ethics Committee of Zhongnan Hospital of Wuhan University under animal protocol number ZN2022266. After being anesthetized by intraperitoneal pentobarbital sodium (1%, 5 mL/kg; Sigma-Aldrich, USA), a hundred male wild-type C57BL/6 mice received the Achilles tendon transection on the left hind limb, as previously described [34].

2.9. In vivo drug degradation study

Three weeks after surgery, HO mice were administrated 100 μL of either WL-808 (5 mg/kg) or IR-808 (2.5 mg/kg) via intravenous injection (n = 3). At different time points post-injection (1 h, 2 h, 6 h, and 12 h), fluorescence images were taken using a Bruker Xtreme BI imaging system (Bruker, USA), with an exposure time of 2 s and the excitation and emission wavelengths of 750 and 790 nm, respectively. The injured tendons at different time points were harvested from the tendon insertion into the calcaneus to the distal gastrocnemius to make paraffin-embedded sections (n = 3). The sections were stained with DAPI and scanned using the CLSM.

2.10. In vivo treatment protocol

To evaluate the prophylactic effect of PDT with WL-808 on HO development, mice were randomly assigned to four groups one-week post-surgery: the WL-808 + 1 W/cm^2 laser group, the IR-808 + 1 W/cm^2 laser group, the laser group and the control group (without any intervention) (n = 9). After 6 h of intravenous injection of either WL-808 (5 mg/kg) or IR-808 (2.5 mg/kg), the Achilles tenotomy sites were irradiated for 2 min (808 nm, 1 W/cm^2) followed by a second round of irradiation 5 min later on ice to eliminate the photothermal effect. The same 808-nm laser device used in cell experiments was used to provide irradiation. The treatment was administered twice a week for 3 weeks. To evaluate the power density-dependent inhibitory effect of PDT with WL-808 on HO formation, other mice were also randomly divided into four groups one-week post-surgery: the WL-808 + 1 W/cm^2 laser group, the WL-808 + 0.5 W/cm^2 laser group, the WL-808 + 0.25 W/cm^2 laser group and the control group (n = 6). To evaluate the therapeutic effect of PDT with WL-808 on HO development after the formation of ectopic cartilage, another group of mice (n = 3) were treated with WL-808 + 1 W/cm^2 laser twice a week for 3 weeks from 4 weeks post-surgery.

2.11. In vivo PDT assessment

After the last irradiation, the HO samples were excised immediately from all groups (n = 3). *In vivo* ROS generation was visualized with a DHE (dihydroethidium) assay kit (Beyotime Biotechnology). Three days after the final irradiation, 3 mice in each group were sacrificed and the left hind limbs were collected for Safranin O red/fast green (SOFG) staining to evaluate ectopic cartilage formation. Immunohistochemical staining of the collagen II, MMP-9 and MMP-13 with respective antibodies was also conducted. The relevant information about all primary antibodies is listed in Table S2. A TUNEL assay (Roche, Switzerland) was performed to assess cell apoptosis in the ectopic cartilage lesions. Major organs from both the WL-808 + laser and control groups were harvested and stained with H&E. At 10 weeks after surgery, Masson's Trichrome staining was performed to evaluate the ectopic bone formation (n = 3). High-resolution micro-CT scans of the left hind limbs were also performed using a micro-CT system (SkyScan 1176; Bruker microCT, Belgium) to examine the volume of HO.

2.12. Bioinformatics analysis

Three days after the last treatment, the HO samples in control and WL-808 + 1 W/cm^2 laser groups were collected for total RNA extraction (n = 3). The transcriptome was sequenced using the Illumina sequencing platform. DEGs were analyzed using the DESeq R package (1.10.1). In addition, potential functions of the DEGs were predicted by KEGG pathway analyses.

2.13. Statistical analysis

All relevant data are presented as mean ± standard deviation (SD), and GraphPad Prism 8.3 (GraphPad Software., USA) was used for data analysis. Student's t-test was employed to compare the quantitative data between the two groups. Comparisons among the groups were analyzed using the one-way ANOVA analysis of variance followed by Tukey's post hoc test. Statistical significance was assigned for $P < 0.05$ ($^*P < 0.05$, $^{**}P < 0.01$, $^{***}P < 0.001$).

3. Results

3.1. Characterization and single oxygen production of WL-808

The influence of the WYRGRL on the optical properties of IR-808 was studied. The maximum emission wavelength of WL-808 and IR-808 in FBS were 814 nm and 813 nm, respectively, while their maximum absorption wavelengths were 798 nm and 796 nm, respectively (Fig. 1A). These results showed that WL-808 and IR-808 displayed similar fluorescence excitation and emission patterns.

As a photosensitizer, the photodynamic characteristics of IR-808 are critical for therapeutic effects. Herein, to assess the photodynamic property of WL-808, we evaluated the production of $^1O_2$ with a SOSG probe. The fluorescence intensity of SOSG in WL-808 and IR-808 was remarkably higher than that in blank PBS (Fig. 1B), indicating that WL-808 could theoretically serve as a photosensitizer for PDT applications. However, the fluorescence intensity of SOSG in WL-808 was lower than that in IR-808. The reason for this phenomenon is unknown, but we speculated that the introduction of WYRGRL might change some functional groups of IR-808 and ultimately lead to the weakened ability to produce $^1O_2$ of WL-808.

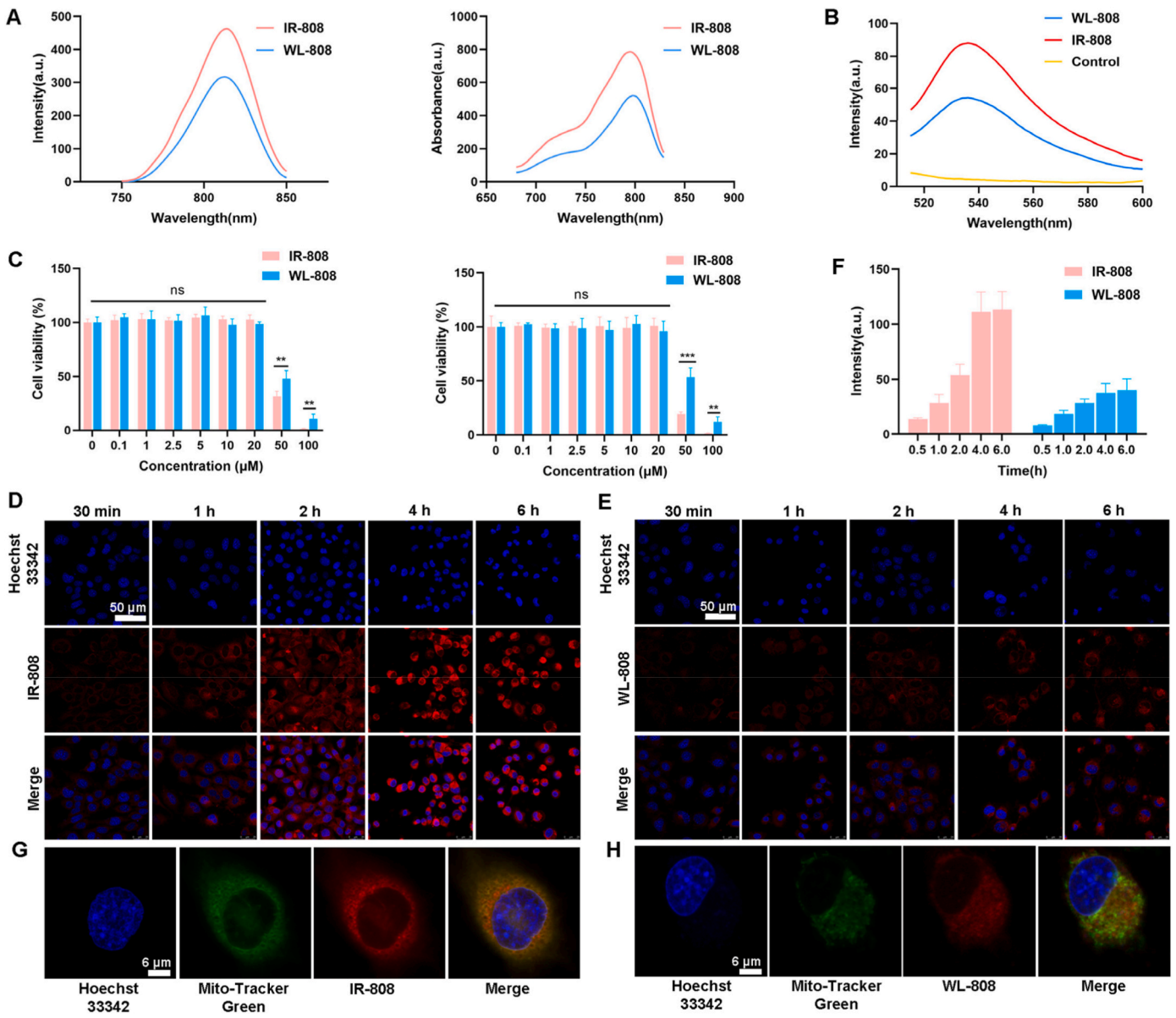

Fig. 1. The optical properties and cellular uptake of WL-808. (A) The absorption and emission spectra of WL-808 and IR-808 in FBS. (B) The fluorescence signal of SOSG. (C) Cell viability of chondrocytes upon treatment with different formulations in the dark. (D, E) CLSM images of chondrocytes cultured with WL-808 and IR-808 at different time points (0.5–6 h). (F) Statistics of mean fluorescence intensity of WL-808 and IR-808. (G, H) Mitochondrial localization of WL-808 and IR-808 in chondrocytes by co-staining with Mito-tracker Green. Data were shown as mean ± SD, n = 3. ns: not significant. CLSM: confocal laser scanning microscope. (For interpretation of the references to color in this figure legend, the reader is referred to the Web version of this article.)

3.2. *In vitro* dark cytotoxicity

Before conducting further cell experiments, we evaluated the dark cytotoxicity of WL-808 and IR-808 on chondrocytes with different concentrations (0–100 μM) after 24 h or 48 h of incubation. Both WL-808 and IR-808 showed no significant cytotoxicity up to 20 μM (Fig. 1C). As the concentration increased from 50 μM to 100 μM, IR-808 and WL-808 generated obvious cytotoxicity. Therefore, the following *in vitro* experiments were conducted at concentrations below 20 μM.

3.3. Cellular uptake and localization

The uptake behavior of WL-808 and IR-808 by chondrocytes showed a positive correlation with time (Fig. 1D–F), which is highly advantageous to generate singlet oxygen in the cells. Furthermore, IR808 has a stronger uptake ability than WL-808, which might be attributed to the better lipid solubility of the IR-808 than WL-808 (CLogP: 8.585 vs. 4.132) or the introduction of WYRGRL increasing the molecular mass and changing the functional groups of IR-808. Mitochondria play a central role in producing reactive oxygen species as byproducts of metabolism and energy production. The mitochondrial targeting property of WL-808 and IR-808 was investigated using a mitochondrial tracker (Fig. 1G and H). Pearson's correlation factors for WL-808 and IR-808 were 0.752 and 0.972, respectively. The high overlap of the red fluorescence of WL-808 with the green fluorescence of Mito-tracker indicated that WL-808 has an ideal mitochondrial targeting property.

3.4. Intracellular ROS generation

The PDT efficacy depends on ROS generation. Herein, the intracellular ROS generation was first evaluated by DCFH-DA, which would be converted to the fluorescent DCF (green) by the generated ROS. The WL-

808 + 1 W/cm^2 laser and IR-808 + 1 W/cm^2 laser groups both showed significantly higher ROS generation than the non-laser irradiation groups and single laser irradiation group, as revealed by CLSM images (Fig. 2A and B). Furthermore, the chondrocytes morphology also responded to the differences in ROS production. In the non-laser irradiation groups and single laser irradiation group, chondrocytes displayed a healthy morphology. In contrast, chondrocytes in the WL-808 + laser and IR-808 + laser groups presented the dying feature of retracting "blebs" due to excessive ROS production. Similar to the results of single oxygen production, ROS induced by WL-808 was also less than that induced by IR-808 in chondrocytes, again demonstrating that the introduction of targeted peptides could reduce the photodynamic effect of the parent photosensitizer -IR-808.

3.5. *In vitro* PDT efficacy

The efficacy of PDT with WL-808 for inducing chondrocyte apoptosis was evaluated using flow cytometry with Annexin V and PI staining (Fig. 2C). Chondrocytes in these groups had less than 5% apoptosis rate without laser irradiation, which further signified the excellent biocompatibilities of WL-808. After irradiation, chondrocytes in different groups had significantly different apoptosis rates. Single laser irradiation did not affect cell viability, indicating that the 808 nm light shows no obvious negative impact on the cells. The PDT effects of IR-808 and WL-808 both have strong cell-killing effects, and the apoptosis rate significantly increased to 94.8% and 53.3%, respectively (Fig. 2D). Then, the PDT effect of WL-808 on chondrocyte viability was further assessed by co-staining with calcein AM (live cells) and PI (dead cells). The intensity of the red fluorescence from PI, indicating the dead cells, was stronger in the WL-808 + laser and IR-808 + laser groups than in the non-laser irradiation groups and single laser irradiation group (Fig. 2E and CF). Furthermore, tremendous ROS generation in the WL-808 + laser group further enhanced the expression of cleaved Caspase-3 and Bax, and suppressed Bcl-2 expression, implying enhanced mitochondria-mediated apoptosis (Fig. 2G–J). Together, these results demonstrated that WL-808 could effectively induce ROS overload-mediated apoptosis and inhibit cell viability, although the introduction of WYRGRL reduces the photodynamic properties of the parent photosensitizer-IR-808.

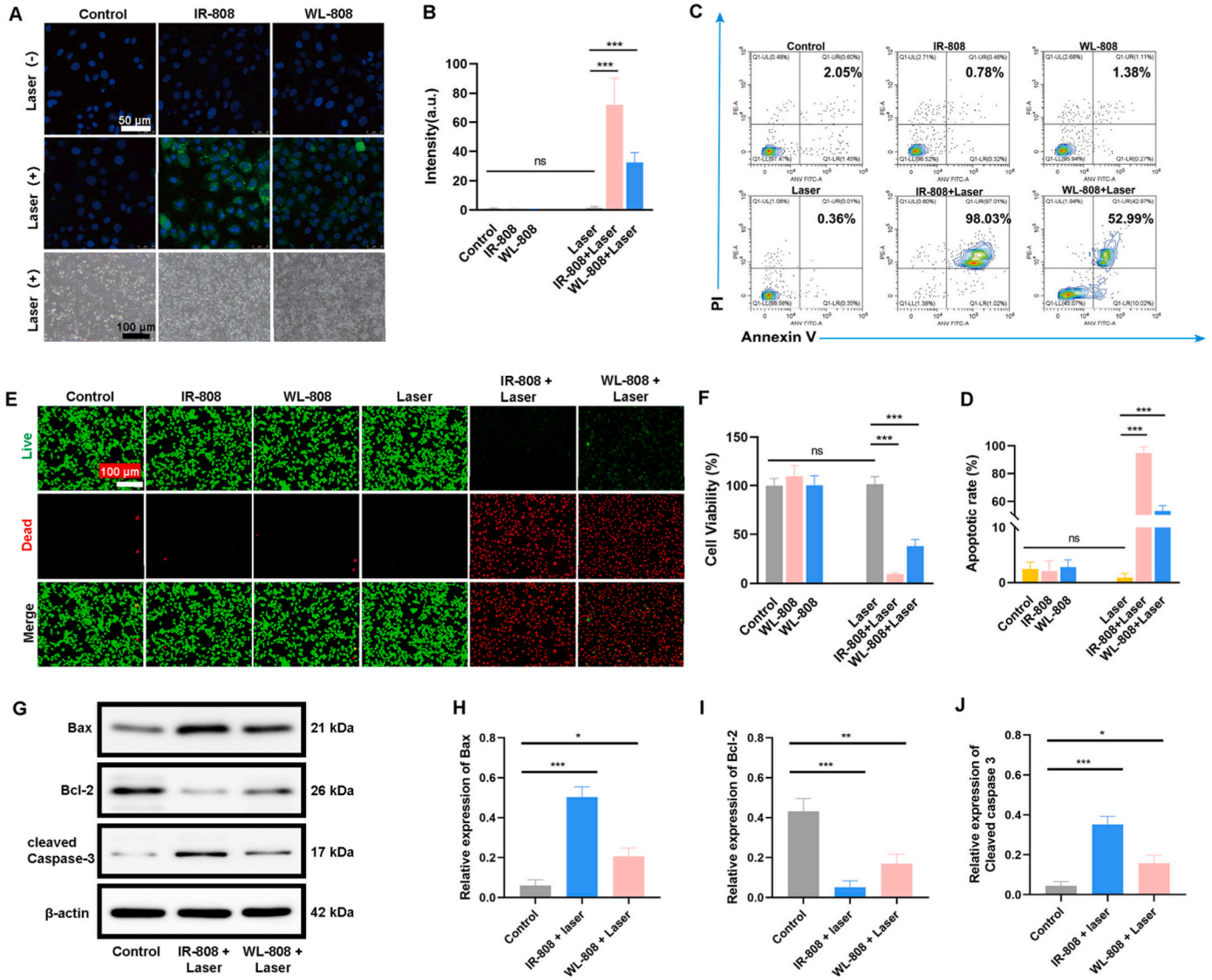

Fig. 2. *In vitro* PDT efficacy of WL-808. (A) CLSM results of intracellular ROS levels and white light images of chondrocytes in different groups after laser irradiation. (B) Statistical analysis of intracellular ROS levels. (C) Flow cytometry results of chondrocytes apoptosis under different treatments for 24 h. (D) Statistical analysis of chondrocytes apoptosis. (F) Fluorescent images of chondrocytes stained with calcein AM and PI after various treatments for 24 h. (G) Cell viability of chondrocytes after various treatments for 24 h. (H) Western blot analyses of the expression of Bax, Bcl-2 and cleaved Caspase-3 in chondrocytes under different treatments for 24 h. (I–K) Quantification of the expressions of Bax, Bcl-2 and cleaved Caspase-3 assessed by western blot. Data were shown as mean ± SD, n = 3. ns: not significant.

3.6. WL-808 degradation in vivo

To investigate the degradation of WL-808 in cartilage lesions of HO, Bruker Xtreme BI imaging system was used to observe the fluorescence signal in the injury sites at different time points post-injection (1 h, 2 h, 6 h and 12 h). The NIR fluorescence intensity of the injury site in the WL-808 group gradually increased and peaked at 6 h post-injection. Then, a decline of fluorescence intensity over time indicated gradual degradation of WL-808 (Fig. 3A). CLSM images also showed that WL-808 adhered to the cartilage lesions of HO and could accumulate in chondrocytes after intravenous injection of WL-808 (Fig. 3B and C). However, no obvious fluorescence was observed at the injured site after injection of IR-808 both *in vivo* and ex vivo. Even though the above results showed that the photodynamic effect of IR-808 was better than that of WL-808, IR-808 could not target the cartilage lesions of HO. During the chondrogenic phase of HO formation, the cartilage matrix molecules like collagen types II and X and aggrecan are produced, while the collagen type II expression is not detected in normal Achilles tendons [10]. Thus, WL-808 cannot be deposited in the healthy tendon, and the fluorescence was not observed in the contralateral Achilles tendon. For

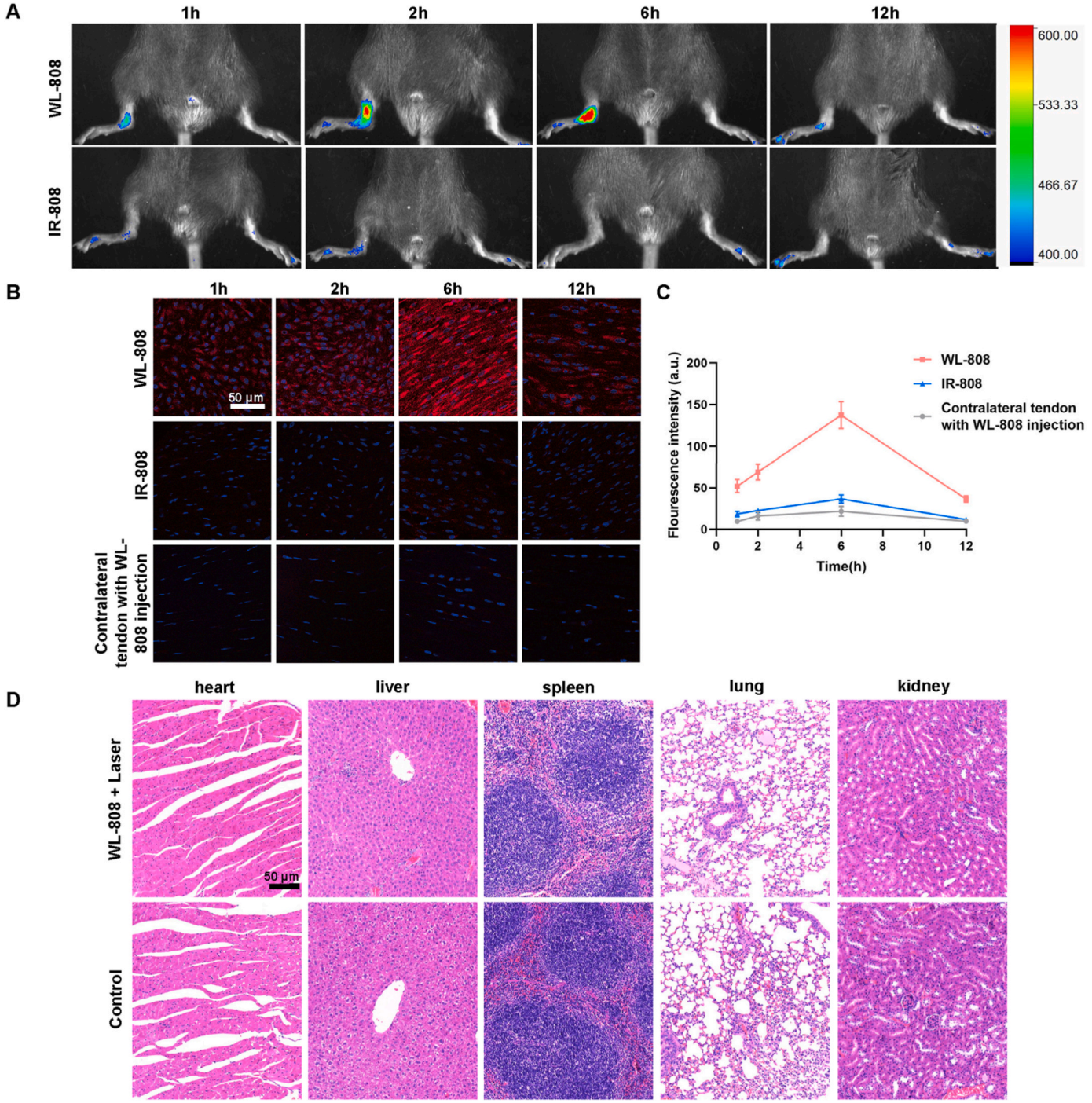

Fig. 3. *In vivo* assessment of ectopic cartilage-affinity ability of WL-808 in tendon HO model mice. (A) Representative fluorescence images of WL-808 absorption and degradation in cartilage lesions of HO at different time points post-injection. (B) CLSM images of HO samples and contralateral healthy Achilles tendon post-injection. (C) Quantitative analysis of average NIR intensity in HO samples and contralateral healthy Achilles tendon post-injection. (D) H&E staining results of major organs harvested from mice after the last injection of WL-808. Data were shown as mean ± SD, n = 3.

the *in vivo* toxicity of WL-808, H&E staining of the major organs harvested at 4 weeks post-surgery indicated no apparent damage or inflammation compared with the control group (Fig. 3D). Taken together, WL-808 could effectively target and accumulate to the ectopic cartilage with good biological safety, which is expected to serve as an effective photosensitizer suitable for HO-targeted PDT.

3.7. *In vivo* PDT efficacy on HO model mice

Encouraged by the promising *in vitro* performance of WL-808, we further selected an Achilles tenotomy mouse model to evaluate its *in vivo* PDT efficacy on HO formation (Fig. 4A). Temperature measurements at the Achilles tenotomy sites showed no significant difference between

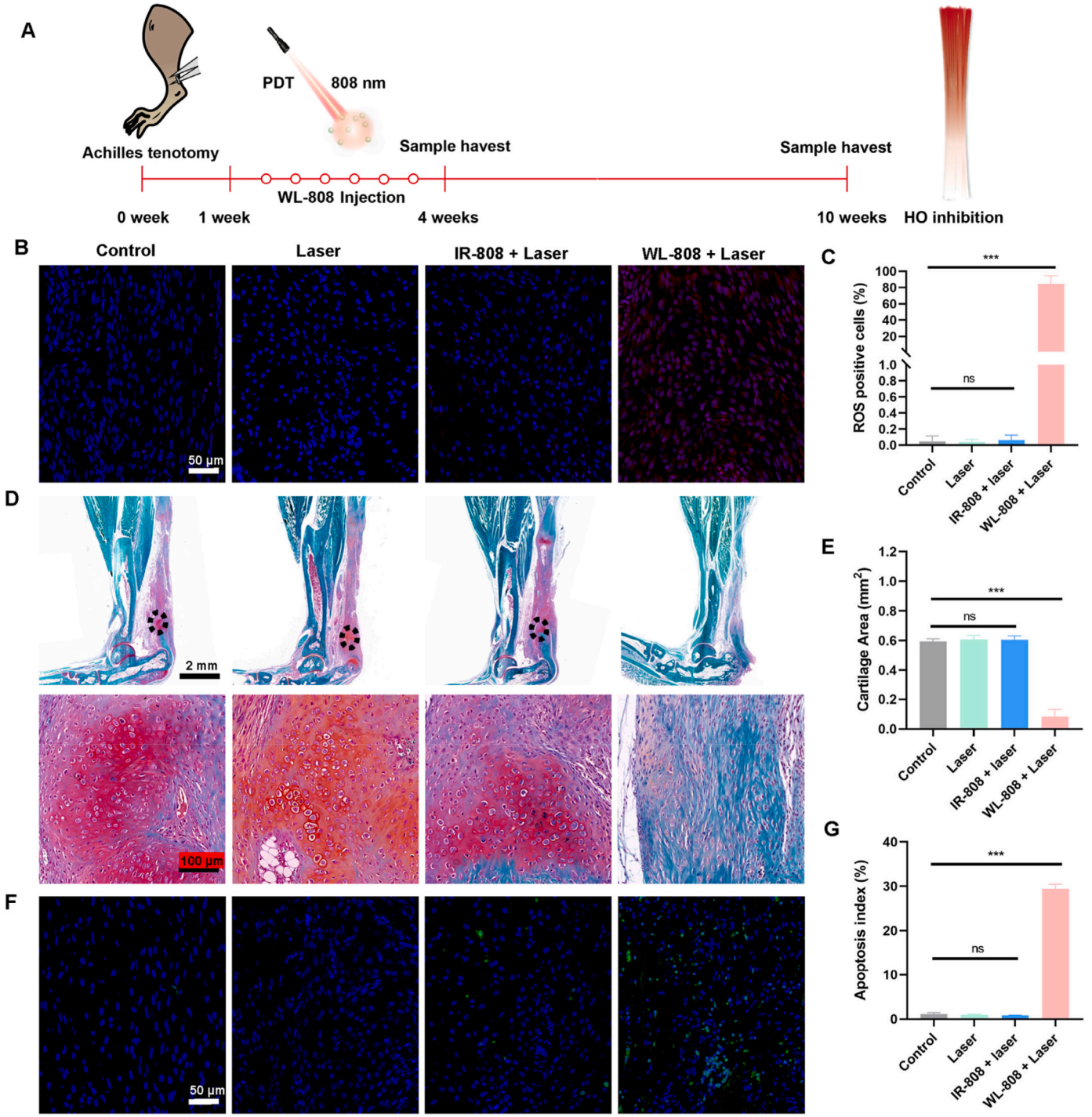

Fig. 4. PDT with WL-808 inhibited ectopic cartilage formation in HO model mice. (A) Schematic illustration of the animal experimental procedure. (B) *In vivo* ROS generation detected by a DHE assay kit in HO tissue. (C) Statistical analysis of *in vivo* ROS levels. (D) Representative SOFG staining images within the lesion site from control, laser, IR-808 + 1 W/cm^2 laser and WL-808 + 1 W/cm^2 laser groups at 4 weeks after tenotomy. The black circle indicated the ectopic cartilage. Original magnification: × 1 (top row); × 20 (bottom row). (E) Histomorphometry quantifications of ectopic cartilage areas in the lesion sites. (F) TUNEL staining of HO tissues. (G) Apoptosis index (TUNEL-positive cells/total cell number [DAPI]) in each group. ns: not significant. Data were shown as mean ± SD, n = 3. ns: not significant. DHE: dihydroethidium. SOFG: Safranin O red/Fast green. (For interpretation of the references to color in this figure legend, the reader is referred to the Web version of this article.)

different groups after irradiation (Fig. S1), thus ruling out the possibility of a PTT effect of WL-808. We then analyzed the *in vivo* ROS generation immediately after the last irradiation using the DHE assay kit. Obvious red fluorescence of DHE was observed only at the tendon injury site in the WL-808 + laser group (Fig. 4B and C), indicating the high specificity for targeting the HO cartilage lesions and the ideal photodynamic effect of WL-808. Subsequent SOFG staining of the lesion tissue sections at 4 weeks post-surgery revealed a significant decrease in cartilage areas in the WL-808 + laser group compared to the control group (Fig. 4D and E). In contrast, single irradiation or irradiation with IR-808 had no effect on the formation of cartilage lesions, further indicating that WL-808 had HO-targeted therapeutic ability while IR-808 did not. In addition, the cell apoptosis rate in the HO tissues was also investigated using TUNEL assays. The results demonstrated that PDT with WL-808 caused substantially increased cell apoptosis within the HO tissues from mice in the WL-808 + laser group compared to the other three groups (Fig. 4F and G). Taken together, we hypothesized that the ROS-based PDT by WL-808 could be effective in HO prophylaxis and treatment because it would target the chondrogenic steps of HO and induce chondrocyte apoptosis.

Subsequently, to explore the specific molecular mechanism of PDT for HO inhibition, differentially expressed genes (DEGs) were identified and Kyoto Encyclopedia of Genes and Genomes (KEGG) analysis was performed to clarify the differences in signaling pathways between the control and WL-808 + laser groups. The results showed 473 down-regulated genes and 105 up-regulated genes in the WL-808 + laser group (fold change ≥2, p-value <0.05) (Fig. 5A–C). A subsequent comparison of the gene expression differences between the WL-808 + laser and control groups and KEGG analysis (Fig. 5D) revealed alterations in the p53 and PI3K-Akt signaling pathways reportedly involved in apoptosis mediated by ROS [35,36]. We further verified whether WL-808/PDT could regulate ROS-related proteins by western blotting. WL-808/PDT increased the protein level of p53 while decreasing that of *p*-Akt and PI3K (Fig. 5 E-H). Overall, the results further indicated that PDT with WL-808 could induce cell apoptosis to inhibit HO formation via regulating ROS-related apoptosis pathways.

Furthermore, collagen II, an important component of ECM in HO cartilage lesion, was also examined by immunohistochemistry (Fig. 6A). Extensive deposition of collagen II was observed in the control group, but significantly reduced after PDT with WL-808 (Fig. 6B). Moreover, the expressions of MMP-9 and MMP-13, which influence collagen metabolism, were also evaluated using immunohistochemistry staining (Fig. 6C–F). The increased expression of MMP-9 and MMP-13 was proportional to enhanced PDT based on quantifying analysis, confirming that PDT with WL-808 could promote ECM degradation of ectopic cartilage *in vivo*. As ECM serves as the important template for mineralization, degradation of ECM might lead to the inhibition of the final ectopic bone formation.

The final measurement of ectopic bone formation is crucial for

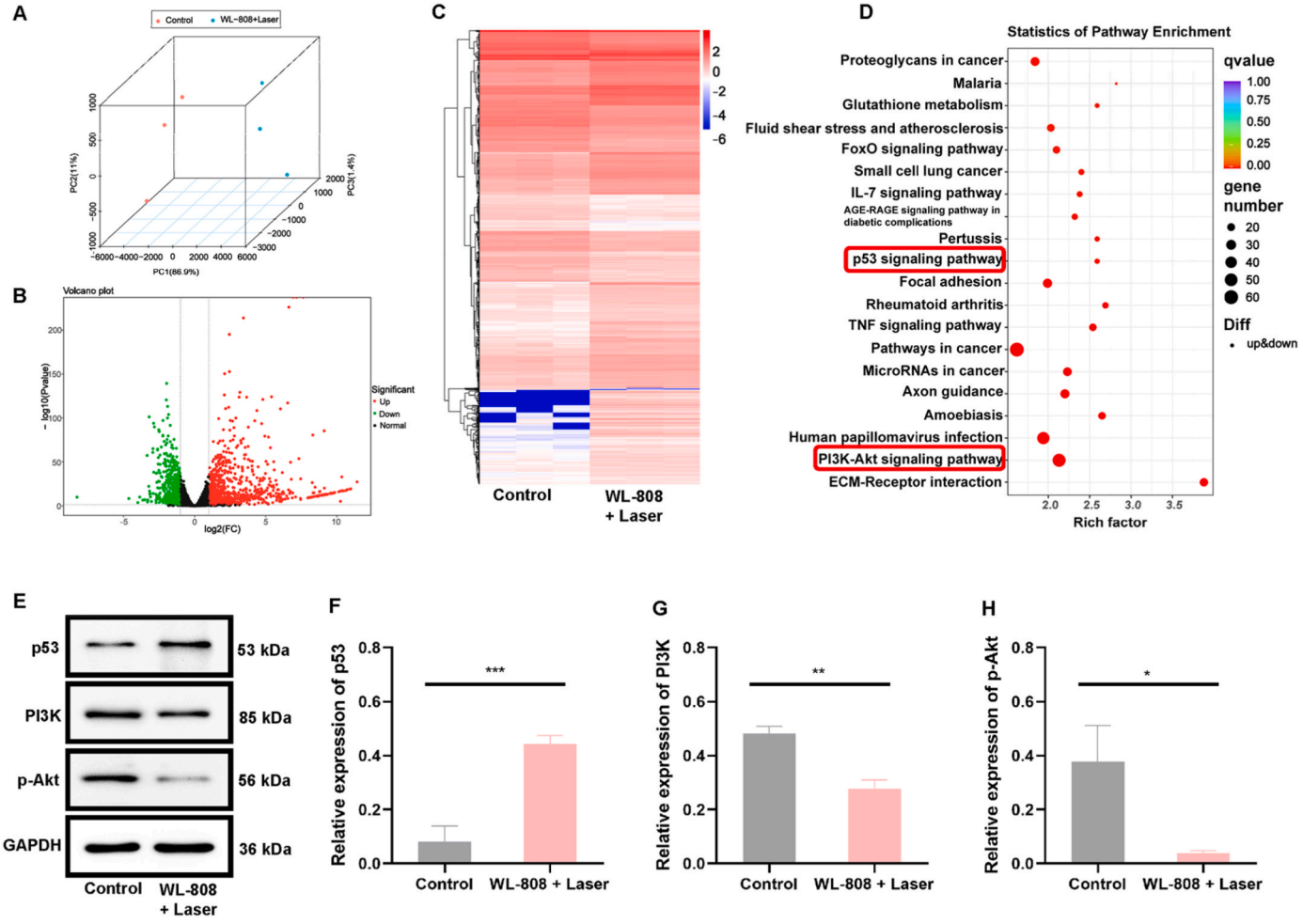

Fig. 5. Bulk-RNA-seq results and western blot analyses of the cartilage lesions of HO from WL-808 + 1 W/cm^2 laser and control groups. (A) Principal component analyses (PCA) of RNA-seq showed that the control group and WL-808 + 1 W/cm^2 laser group were significantly distinguished from each other. (B) Volcano plot of the DEGs. (C) Clustering analysis of the DEGs. (D) Significantly upregulated signaling pathways in different biological processes of KEGG classification in the WL-808 + laser group vs. the control group. (E) Western blot analyses of p53, PI3K and *p*-Akt expression in the tendon injury sites between the WL-808 + laser group and the control group. (F–H) Quantification of the expressions of p53, PI3K and *p*-Akt assessed by western blot. Data were shown as mean ± SD, n = 3.

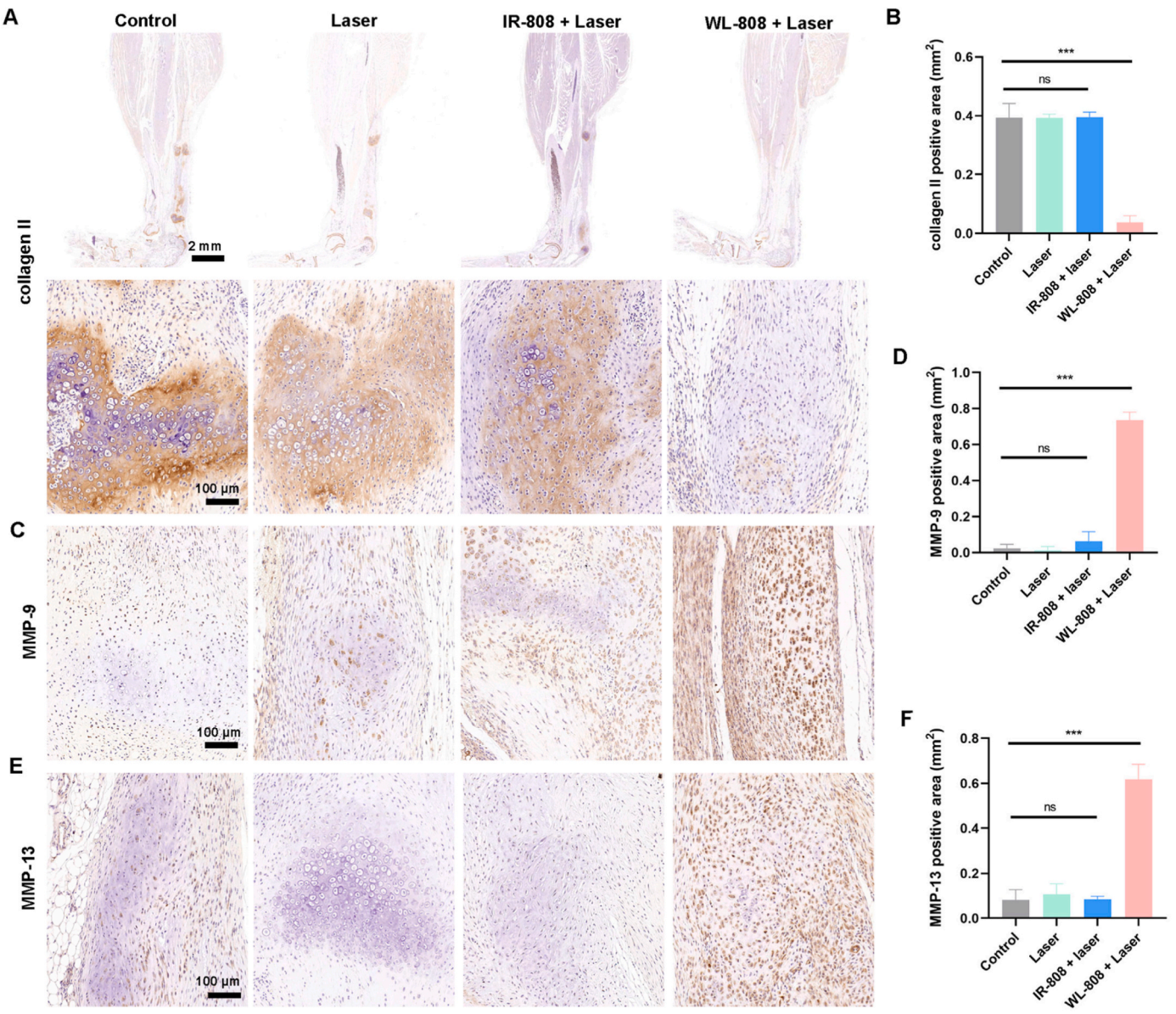

Fig. 6. PDT with WL-808 promoted extracellular matrix degradation of ectopic cartilage in HO model mice. (A, C, E) Immunohistochemical analyses of collagen II, MMP-9 and MMP-13 expressions in HO tissues. (B, D, F) Statistical analysis of collagen II, MMP-9 and MMP-13 expressions. Data were shown as mean ± SD, n = 3. ns: not significant.

evaluating the prophylactic effect. Thus, Masson's trichrome staining was performed on samples taken 10 weeks after tenotomy to highlight the ectopic bone matrix. The WL-808 + 1 W/cm^2 laser group showed a less conspicuous ectopic bone matrix compared to the other three groups (Fig. 7A). Additionally, micro-CT revealed a significant reduction in ectopic bone volume in the WL-808 + 1 W/cm^2 laser group (Fig. 7B and C). Moreover, treating with PDT assisted by WL-808 resulted in a power density-dependent decrease in ectopic cartilage (Fig. 8A and B) and bone formation (Fig. 8C–E) after tenotomy at the power densities from 0.25 W/cm^2 to 1 W/cm^2, which could be attributed to the fact that ROS generation increased with the enhanced irradiation. Taken together, PDT with WL-808 triggers cell apoptosis in ectopic cartilage lesions through ROS-mediated oxidative stress and thus exerts an ideal effect on suppressing eventual HO formation. We also tested the effects of PDT with WL-808 on ectopic bone formation in mice with ectopic cartilage developed via Achillotomy for 4 weeks. Masson's trichrome staining (Fig. S2A) and micro-CT analysis (Fig. S2B) revealed that PDT with WL-808 could notably inhibit ectopic bone formation, suggesting that treatment with PDT with WL-808 at later stages of cartilage formation could also significantly suppress eventual HO formation.

4. Discussion

HO is an intractable sequela caused by pathological chondrogenic and osteogenic differentiation of tissue-resident mesenchymal progenitor cells (TMPCs) and subsequent deposition of the bone and cartilage matrix at extraskeletal sites [1]. During HO formation, chondrocytes firstly proliferate, undergo hypertrophy and death; the cartilage extracellular matrix is mineralized; finally osteoblast differentiation leads to replacement of the cartilage tissue with bone [10]. Inhibiting or minimizing HO formation by targeting the early phase of cartilage formation has been shown to be effective [15]. Previously, we assessed the potential of a near-infrared probe, WL-808, for early diagnosis of HO by targeting ectopic cartilage lesions [31]. In this study, we aimed to evaluate the therapeutic potential of WL-808 for the innovative HO-PDT approach. We have demonstrated for the first time that PDT with

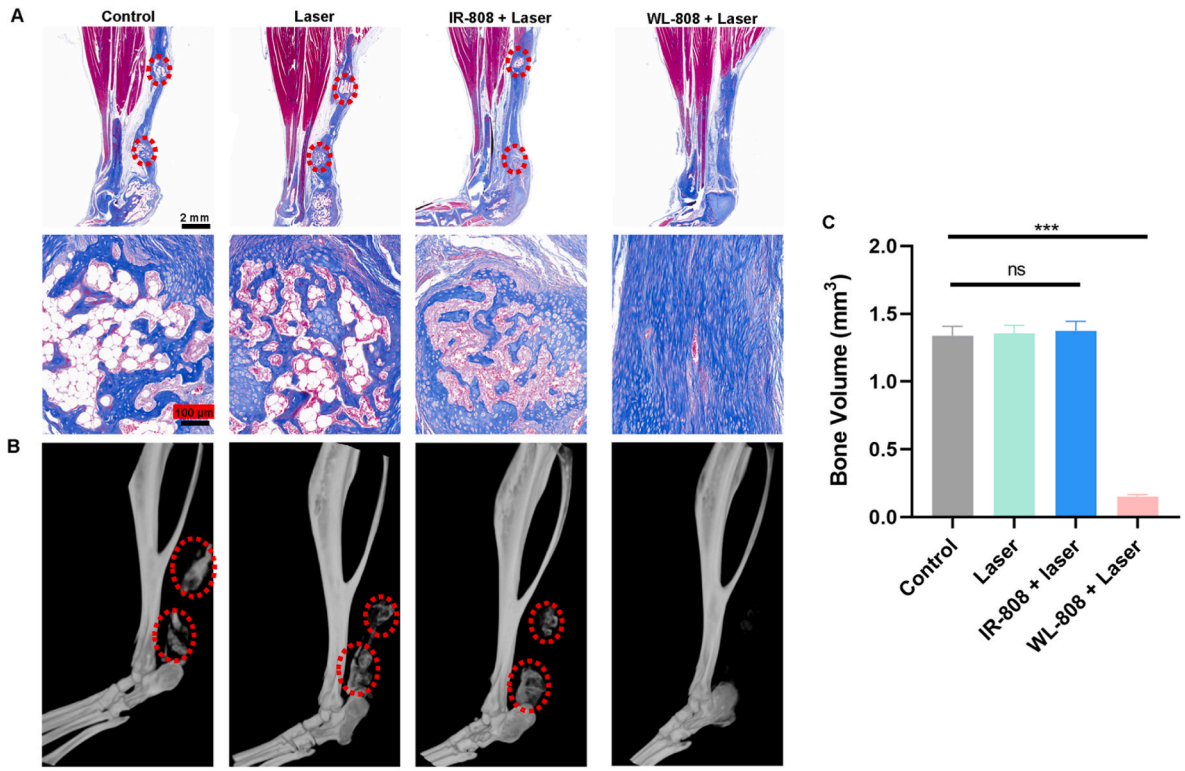

Fig. 7. Treatment with PDT assisted by WL-808 at the early stage of cartilage formation has inhibiting effects on ectopic bone formation. (A) Masson's trichrome staining within the lesion site from different groups 10 weeks after tenotomy. The red circle indicated the ectopic bone. Original magnification: × 1 (top row); × 20 (bottom row). (B) Micro-CT reconstruction images of ectopic bone formation (red circle) from different groups at 10 weeks after tenotomy. (C) Micro-CT quantifications of ectopic bone volume in the lesion sites. Data were shown as mean ± SD, n = 3. ns: not significant. (For interpretation of the references to color in this figure legend, the reader is referred to the Web version of this article.)

WL-808 could inhibit the development of tendon HO via inducing chondrocyte apoptosis and ECM degradation in ectopic cartilage lesions.

PDT is a promising non-invasive treatment option for various proliferative diseases, such as malignant carcinomas and hypertrophic scars [17–26]. IR-808 has been reported to exhibit excellent photodynamic properties for tumor therapy via generating ROS [32]. However, IR-808 lacks specificity in HO lesions. Similar to the normal articular cartilage, large Col2a1 cartilaginous templates are detected in the tendon injury sites at the proliferative stage of HO formation, making them a potential target for HO treatment. In contrast, type III collagen and type I collagen are the dominant structural components of tendon tissue, while the Col2a1 expression was not detected in healthy tendons [10,11]. In the present study, we aimed to enhance the specificity of IR-808 for ectopic cartilage lesions in HO with the Col2a1-targeting peptide (WYRGRL) modification. Chondrocytes are the critical cells during pathological chondrogenesis, and they initially undergo proliferation and hypertrophy to form a template-cartilage extracellular matrix. For the group treated with WL-808-PDT compared to the control group, elevated intracellular ROS in chondrocytes was found, which correlated with the singlet oxygen detected by the DPBF probe. However, WL-808 exhibited weaker singlet oxygen and intracellular ROS generation than IR-808. We hypothesized that this might be related to the poor lipid solubility of WL-808 leading to less drug entry into chondrocytes or the introduction of WYRGRL increasing the molecular mass and changing the functional groups of IR-808.

A regulated basal level of ROS is essential and advantageous to cell growth and differentiation [37]. For instance, chondrocytes exhibited increased survival after 5-aminolevulinic acid-based PDT (5 J/cm^2) [30]. However, excessive levels of ROS have been considered to induce cellular dysfunction and organismal death via the destructive oxidation of intra-cellular components. In patients with osteoarthritis (OA), ROS levels are significantly higher in the cartilage compared to healthy individuals. ROS-induced oxidative stress contributes to the dysfunction and apoptosis of cartilage-resident chondrocytes and ECM degradation, which exerts a major pathogenic role in the progression of OA [38]. In this study, we investigated the efficacy of PDT using WL-808 on chondrocytes *in vitro*. At a radiation power density of 720 J/cm^2, WL-808 induced significant chondrocyte apoptosis and upregulated apoptosis-specific genes (Bcl-2, Bax, and cleaved-Caspase3) *in vitro*. These findings are important for the *in vivo* application of the WL-808-PDT. Additionally, previous studies have shown that photobiomodulation induced by single irradiation (808 nm; 0.8 J or 1.4 J) increased chondrocyte proliferation and provided chondroprotection [39]. The results of our *in vitro* studies showed no difference in cell viability between the control and laser groups, which might be attributed to differences in radiation power density.

In our *in vivo* study, we observed a significant inhibition of HO formation following treatment with WL-808 both at the early stage of cartilage formation and after the ectopic cartilage had developed under NIR laser irradiation, without any side effects. This presents a practical option for imaging-guided therapy. Similar to the *in vivo* PDT effects, PDT with WL-808 remarkably increased cell apoptosis within the HO tissues. KEGG analysis also revealed that p53 and PI3K-AKT signaling pathways, reportedly involved in ROS-mediated apoptosis, were altered in the WL-808 + laser group. It has been confirmed that p53 activation and PI3K/AKT inactivation can induce cell apoptosis by regulating the downstream mitochondrial apoptotic signaling pathway [35,36,40]. Moreover, western blotting analysis further confirmed that compared to the control group, PDT with WL-808 enhanced the expression of p53 and decreased the expression of PI3K and *p*-AKT in the tendon injury sites. Therefore, we believe that PDT with WL-808 triggers cell apoptosis in ectopic cartilage lesions through ROS-mediated oxidative stress and thus exerts an ideal effect on preventing HO formation.

Matrix metalloproteinases (MMPs) are a major member of the

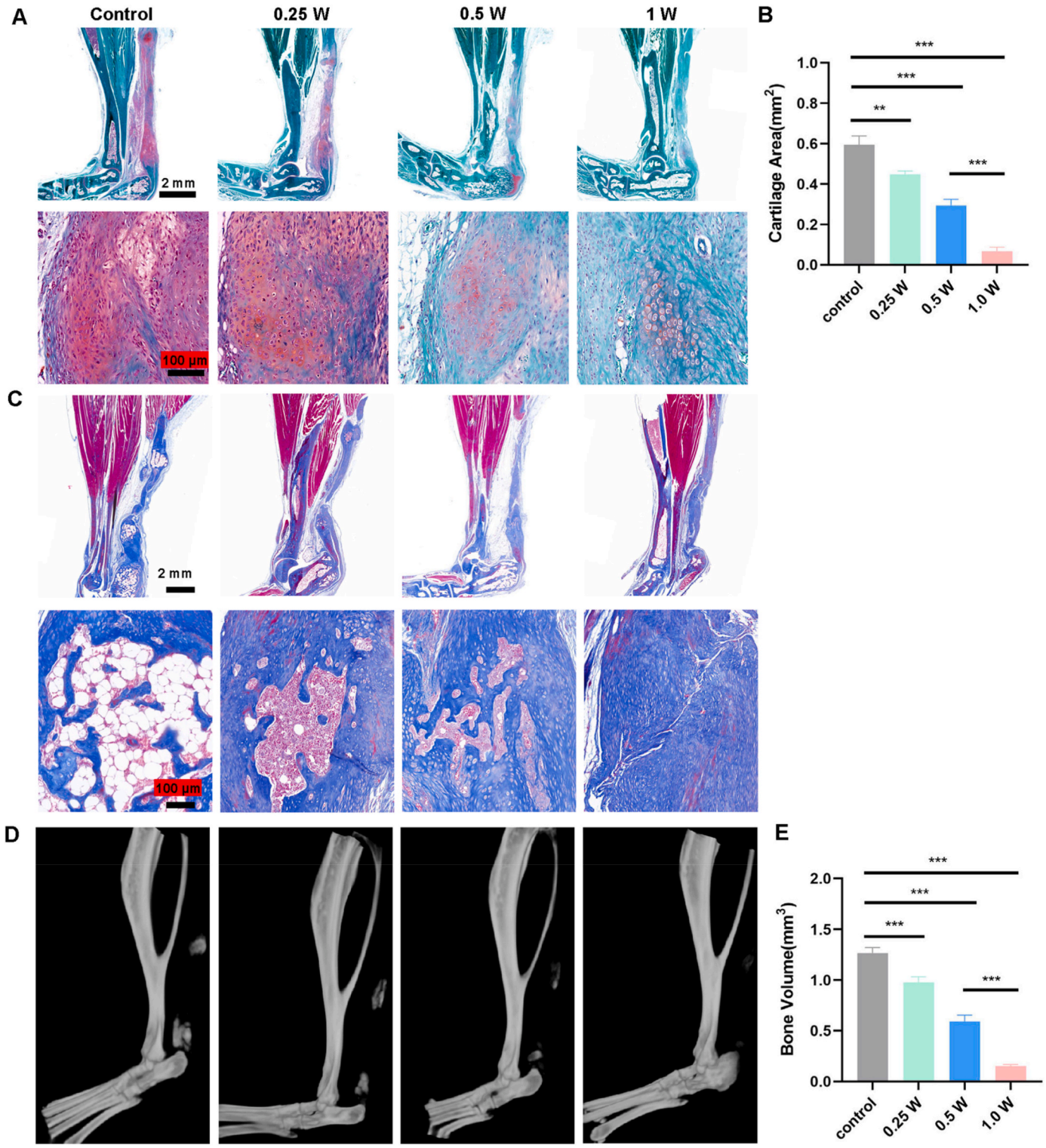

Fig. 8. HO formation treated with control or WL-808 at different laser power densities. (A) Representative SOFG staining images in different groups at 4 weeks after tenotomy. Original magnification: × 1 (top row); × 20 (bottom row). (B) Histomorphometry quantifications of ectopic cartilage areas in the lesion sites. (C) Masson's trichrome staining within the lesion site from different groups 10 weeks after tenotomy. Original magnification: × 1 (top row); × 20 (bottom row). (D) Micro-CT reconstruction images of ectopic bone formation from different groups at 10 weeks after tenotomy. (E) Micro-CT quantifications of ectopic bone volume in the lesion sites. Data were shown as mean ± SD, n = 3. ns: not significant. SOFG: Safranin O red/Fast green. (For interpretation of the references to color in this figure legend, the reader is referred to the Web version of this article.)

proteolytic enzyme family, participating in chondrocyte apoptosis and the degradation of ECM components (aggrecan and collagen II) in cartilage. During the progress of OA, the levels of MMP-9 and MMP-13 significantly increase, resulting in the degradation of articular cartilage [41]. Previous studies have shown that collagen deposition significantly reduces and the expression of MMP-3, which influences collagen metabolism, increases after PDT treatment for hypertrophic scars [18,42]. Interestingly, there were more expressions of MMP-9 and MMP-13 and less expression of collagens II in the tendon injury sites after PDT with WL-808, which were correlated with the formation of smaller cartilage matrixes, indicating that PDT could also enhance ECM degradation of ectopic cartilage. As ECM serves as the important template for mineralization, degradation of ECM leads to the inhibition of the final ectopic bone formation.

Our study had several limitations. First, The ROS generation ability of WL-808 was significantly weaker than that of its parent photosensitizer-IR-808 after the introduction of WYRGRL. We are still committed to developing new cartilage targeting photosensitizers with enhanced ROS generation ability for HO-PDT. The design and synthesis methods of the photosensitizers for tumor PDT therapy may provide us with new ideas to develop photosensitizers with better performance and safety for HO-PDT [20,21,43,44]. Second, in the present study, we only tested the effects of PDT with WL-808 on ectopic bone formation at 1 and 4 weeks after Achillotomy. Whether PDT has a therapeutic effect in the later stages of HO has not been studied. Therefore, future researches are warranted to investigate these problems to accelerate the clinical application of this novel method.

5. Conclusion

WL-808 is an ideal photosensitizer for targeting HO cartilage lesions. Moreover, PDT assisted by WL-808 effectively diminishes ectopic cartilage formation and subsequent bone formation in the tenotomy HO model. This effect appears to be related to the chondrocyte apoptosis and ECM degradation of ectopic cartilage within the early HO formation. Our findings suggest a novel perspective for HO prophylaxis and treatment with PDT by producing excessive ROS.

Credit author statement

Zheng Wang: Conceptualization, Methodology, Software, Formal analysis, Investigation, Writing-Original Draft, Visualization, Funding acquisition. Chao Sun: Methodology, Validation, Investigation, Resources, Writing-Original Draft. Yifeng Yu: Investigation, Software, Formal analysis, Writing-Review & Editing. Dong Zhang: Investigation, Resources, Data Curation, Writing-Review & Editing. Baiwen Qi: Visualization, Validation, Writing-Review & Editing, Resources. Zonghuan Li: Conceptualization, Project administration, Validation, Resources, Supervision, Writing-Review & Editing. Xinzeyu Yi: Conceptualization, Project administration, Validation, Resources, Supervision, Writing-Review & Editing. Aixi Yu: Conceptualization, Project administration, Validation, Resources, Supervision, Writing-Review & Editing, Funding acquisition.

Declaration of competing interest

The authors declare that they have no known competing financial interests or personal relationships that could have appeared to influence the work reported in this paper.

Data availability

Data will be made available on request.

Acknowledgements

This study was supported by the Health Commission of Hubei Province Medical Leading Talent Project (LJ20200405).

Appendix B. Supplementary data

Supplementary data to this article can be found online at https://doi.org/10.1016/j.mtbio.2023.100822.

Appendix A. Supplementary data

Supplementary material associated with this article can be found in the online version.

References

[1] D. Dey, J. Bagarova, S.J. Hatsell, K.A. Armstrong, L. Huang, J. Ermann, A. J. Vonner, Y. Shen, A.H. Mohedas, A. Lee, E.M.W. Eekhoff, A. van Schie, M. B. Demay, C. Keller, A.J. Wagers, A.N. Economides, P.B. Yu, Two tissue-resident progenitor lineages drive distinct phenotypes of heterotopic ossification, Sci. Transl. Med. 8 (2016), https://doi.org/10.1126/scitranslmed.aaf1090, 366ra163.

[2] C.D. Hwang, C.A. Pagani, J.H. Nunez, M. Cherief, Q. Qin, M. Gomez-Salazar, B. Kadaikal, H. Kang, A.R. Chowdary, N. Patel, A.W. James, B. Levi, Contemporary perspectives on heterotopic ossification, JCI Insight 7 (2022), https://doi.org/10.1172/jci.insight.158996.

[3] S. Agarwal, S. Loder, D. Cholok, J. Li, C. Breuler, J. Drake, C. Brownley, J. Peterson, S. Li, B. Levi, Surgical excision of heterotopic ossification leads to Re-Emergence of mesenchymal stem cell populations responsible for recurrence, Stem Cells Transl Med 6 (2017) 799–806, https://doi.org/10.5966/sctm.2015-0365.

[4] M. Milakovic, M. Popovic, S. Raman, M. Tsao, H. Lam, E. Chow, Radiotherapy for the prophylaxis of heterotopic ossification: a systematic review and meta-analysis of randomized controlled trials, Radiother. Oncol. 116 (2015) 4–9, https://doi.org/10.1016/j.radonc.2015.05.022.

[5] M. Joice, G.I. Vasileiadis, D.F. Amanatullah, Non-steroidal anti-inflammatory drugs for heterotopic ossification prophylaxis after total hip arthroplasty: a systematic review and meta-analysis, Bone Joint Lett. J 100-B (2018) 915–922, https://doi.org/10.1302/0301-620X.100B7.BJJ-2017-1467.R1.

[6] C. Meyers, J. Lisiecki, S. Miller, A. Levin, L. Fayad, C. Ding, T. Sono, E. McCarthy, B. Levi, A.W. James, Heterotopic ossification: a comprehensive review, JBMR Plus 3 (2019), e10172, https://doi.org/10.1002/jbm4.10172.

[7] S. Asai, S. Otsuru, M.E. Candela, L. Cantley, K. Uchibe, T.J. Hofmann, K. Zhang, K. L. Wapner, L.J. Soslowsky, E.M. Horwitz, M. Enomoto-Iwamoto, Tendon progenitor cells in injured tendons have strong chondrogenic potential: the CD105-negative subpopulation induces chondrogenic degeneration, Stem Cell. 32 (2014) 3266–3277, https://doi.org/10.1002/stem.1847.

[8] J.R. Peterson, S. De La Rosa, O. Eboda, K.E. Cilwa, S. Agarwal, S.R. Buchman, P. S. Cederna, C. Xi, M.D. Morris, D.N. Herndon, W. Xiao, R.G. Tompkins, P. H. Krebsbach, S.C. Wang, B. Levi, Treatment of heterotopic ossification through remote ATP hydrolysis, Sci. Transl. Med. 6 (2014), https://doi.org/10.1126/scitranslmed.3008810, 255ra132.

[9] J.R. Peterson, S. De La Rosa, H. Sun, O. Eboda, K.E. Cilwa, A. Donneys, M. Morris, S.R. Buchman, P.S. Cederna, P.H. Krebsbach, S.C. Wang, B. Levi, Burn injury enhances bone formation in heterotopic ossification model, Ann. Surg. 259 (2014) 993–998, https://doi.org/10.1097/SLA.0b013e318291da85.

[10] L. Lin, Q. Shen, T. Xue, C. Yu, Heterotopic ossification induced by Achilles tenotomy via endochondral bone formation: expression of bone and cartilage related genes, Bone 46 (2010) 425–431, https://doi.org/10.1016/j.bone.2009.08.057.

[11] M. Delgado Caceres, K. Angerpointner, M. Galler, D. Lin, P.A. Michel, C. Brochhausen, X. Lu, A.R. Varadarajan, J. Warfsmann, R. Stange, V. Alt, C. G. Pfeifer, D. Docheva, Tenomodulin knockout mice exhibit worse late healing outcomes with augmented trauma-induced heterotopic ossification of Achilles tendon, Cell Death Dis. 12 (2021) 1049, https://doi.org/10.1038/s41419-021-04298-z.

[12] C. Hwang, S. Marini, A.K. Huber, D.M. Stepien, M. Sorkin, S. Loder, C.A. Pagani, J. Li, N.D. Visser, K. Vasquez, M.A. Garada, S. Li, J. Xu, C.-Y. Hsu, P.B. Yu, A. W. James, Y. Mishina, S. Agarwal, J. Li, B. Levi, Mesenchymal VEGFA induces aberrant differentiation in heterotopic ossification, Bone Res 7 (2019) 36, https://doi.org/10.1038/s41413-019-0075-6.

[13] E. Schipani, Hypoxia and HIF-1alpha in chondrogenesis, Ann. N. Y. Acad. Sci. 1068 (2006) 66–73, https://doi.org/10.1196/annals.1346.009.

[14] E. Schipani, H.E. Ryan, S. Didrickson, T. Kobayashi, M. Knight, R.S. Johnson, Hypoxia in cartilage: HIF-1alpha is essential for chondrocyte growth arrest and survival, Genes Dev. 15 (2001) 2865–2876, https://doi.org/10.1101/gad.934301.

[15] S. Agarwal, S. Loder, C. Brownley, D. Cholok, L. Mangiavini, J. Li, C. Breuler, H. H. Sung, S. Li, K. Ranganathan, J. Peterson, R. Tompkins, D. Herndon, W. Xiao, D. Jumlongras, B.R. Olsen, T.A. Davis, Y. Mishina, E. Schipani, B. Levi, Inhibition of Hif1α prevents both trauma-induced and genetic heterotopic ossification, Proc. Natl. Acad. Sci. U. S. A. 113 (2016) E338–E347, https://doi.org/10.1073/pnas.1515397113.

[16] L. Lin, Q. Shen, H. Leng, X. Duan, X. Fu, C. Yu, Synergistic inhibition of endochondral bone formation by silencing Hif1alpha and Runx2 in trauma-induced heterotopic ossification, Mol. Ther. 19 (2011) 1426–1432, https://doi.org/10.1038/mt.2011.101.
[17] B. Yin, Q. Qin, Z. Li, Y. Wang, X. Liu, Y. Liu, S. Huan, X. Zhang, G. Song, Tongue cancer tailored photosensitizers for NIR-II fluorescence imaging guided precise treatment, Nano Today 45 (2022), 101550, https://doi.org/10.1016/j.nantod.2022.101550.
[18] Y. Huang, T. Peng, W. Hu, X. Gao, Y. Chen, Q. Zhang, C. Wu, X. Pan, Fully armed photodynamic therapy with spear and shear for topical deep hypertrophic scar treatment, J. Contr. Release 343 (2022) 408–419, https://doi.org/10.1016/j.jconrel.2022.01.043.
[19] K. Guan, P. Wang, F. Zhou, Y. Wang, H.-W. Liu, Q. Xie, G. Song, X. Yin, S. Huan, X.-B. Zhang, A two-photon fluorescence self-reporting black phosphorus nanoprobe for the in situ monitoring of therapy response, Chem. Commun. 56 (2020) 14007–14010, https://doi.org/10.1039/d0cc05335j.
[20] P. Wang, F. Zhou, K. Guan, Y. Wang, X. Fu, Y. Yang, X. Yin, G. Song, X.-B. Zhang, W. Tan, In vivo therapeutic response monitoring by a self-reporting upconverting covalent organic framework nanoplatform, Chem. Sci. 11 (2019) 1299–1306, https://doi.org/10.1039/c9sc04875h.
[21] Y. Wang, G. Song, S. Liao, Q. Qin, Y. Zhao, L. Shi, K. Guan, X. Gong, P. Wang, X. Yin, Q. Chen, X.-B. Zhang, Cyclic amplification of the afterglow Luminescent nanoreporter Enables the prediction of anti-cancer Efficiency, Angew Chem. Int. Ed. Engl. 60 (2021) 19779–19789, https://doi.org/10.1002/anie.202104127.
[22] S. Liao, Y. Wang, Z. Li, Y. Zhang, X. Yin, S. Huan, X.-B. Zhang, S. Liu, G. Song, A novel afterglow nanoreporter for monitoring cancer therapy, Theranostics 12 (2022) 6883–6897, https://doi.org/10.7150/thno.77457.
[23] Y. Liu, L. Teng, X.-F. Lou, X.-B. Zhang, G. Song, "Four-In-One" design of a Hemicyanine-based modular scaffold for high-contrast activatable molecular afterglow imaging, J. Am. Chem. Soc. 145 (2023) 5134–5144, https://doi.org/10.1021/jacs.2c11466.
[24] Y. Ma, J. Shang, L. Liu, M. Li, X. Xu, H. Cao, L. Xu, W. Sun, G. Song, X.-B. Zhang, Rational design of a double-Locked photoacoustic probe for precise in vivo imaging of cathepsin B in atherosclerotic plaques, J. Am. Chem. Soc. 145 (2023) 17881–17891, https://doi.org/10.1021/jacs.3c04981.
[25] C. Lu, Z. Li, N. Wu, D. Lu, X.-B. Zhang, G. Song, Tumor microenvironment-tailored nanoplatform for companion diagnostic applications of precise cancer therapy, Chem (2023), https://doi.org/10.1016/j.chempr.2023.06.011.
[26] P. Wang, F. Zhou, X. Yin, Q.J. Xie, G.S. Song, X.B. Zhang, Nanovoid-confinement and click-activated nanoreactor for synchronous delivery of prodrug pairs and precise photodynamic therapy, Nano Res. 15 (2022) 9264–9273, https://doi.org/10.1007/s12274-022-4615-9.
[27] Z. Jiang, H. Wang, Z. Zhang, J. Pan, H. Yuan, Cartilage targeting therapy with reactive oxygen species-responsive nanocarrier for osteoarthritis, J. Nanobiotechnol. 20 (2022) 419, https://doi.org/10.1186/s12951-022-01629-w.
[28] C. Zhu, S. Han, X. Zeng, C. Zhu, Y. Pu, Y. Sun, Multifunctional thermo-sensitive hydrogel for modulating the microenvironment in Osteoarthritis by polarizing macrophages and scavenging RONS, J. Nanobiotechnol. 20 (2022) 221, https://doi.org/10.1186/s12951-022-01422-9.
[29] M. Arra, G. Swarnkar, K. Ke, J.E. Otero, J. Ying, X. Duan, T. Maruyama, M.F. Rai, R.J. O'Keefe, G. Mbalaviele, J. Shen, Y. Abu-Amer, LDHA-mediated ROS generation in chondrocytes is a potential therapeutic target for osteoarthritis, Nat. Commun. 11 (2020) 3427, https://doi.org/10.1038/s41467-020-17242-0.
[30] J.D. Bastian, R.J. Egli, R. Ganz, W. Hofstetter, M. Leunig, Differential response of porcine osteoblasts and chondrocytes in cell or tissue culture after 5-aminolevulinic acid-based photodynamic therapy, Osteoarthritis Cartilage 17 (2009) 539–546, https://doi.org/10.1016/j.joca.2008.08.005.
[31] Z. Wang, X. Yi, W. Yi, C. Jian, B. Qi, Q. Liu, Z. Li, A. Yu, Early diagnosis of heterotopic ossification with a NIR fluorescent probe by targeting type II collagen, J. Mater. Chem. B 11 (2023) 1684–1691, https://doi.org/10.1039/d2tb02157a.
[32] X. Tan, S. Luo, D. Wang, Y. Su, T. Cheng, C. Shi, A NIR heptamethine dye with intrinsic cancer targeting, imaging and photosensitizing properties, Biomaterials 33 (2012) 2230–2239, https://doi.org/10.1016/j.biomaterials.2011.11.081.
[33] W. Tang, J. Kang, L. Yang, J. Lin, J. Song, D. Zhou, F. Ye, Thermosensitive nanocomposite components for combined photothermal-photodynamic therapy in liver cancer treatment, Colloids Surf. B Biointerfaces 226 (2023), 113317, https://doi.org/10.1016/j.colsurfb.2023.113317.
[34] Z. Wei, S. Guo, H. Wang, Y. Zhao, J. Yan, C. Zhang, B. Zhong, Comparative proteomic analysis identifies differentially expressed proteins and reveals potential mechanisms of traumatic heterotopic ossification progression, J Orthop Translat 34 (2022) 42–59, https://doi.org/10.1016/j.jot.2022.04.003.
[35] M.A. Hossain, M.J. Alam, B. Kim, C.-W. Kang, J.-H. Kim, Ginsenoside-Rb1 prevents bone cartilage destruction through down-regulation of p-Akt, p-P38, and p-P65 signaling in rabbit, Phytomedicine 100 (2022), 154039, https://doi.org/10.1016/j.phymed.2022.154039.
[36] M. Chang, X. Ma, T. Ouyang, J. Lin, J. Liu, Y. Xiao, H. Chen, J. Yu, Y. Huang, M. Xu, Potential molecular mechanisms involved in 5-aminolevulinic acid-based photodynamic therapy against Human hypertrophic scars, Plast. Reconstr. Surg. 136 (2015) 715–727, https://doi.org/10.1097/PRS.0000000000001626.
[37] S. Sart, L. Song, Y. Li, Controlling redox status for stem cell survival, Expansion, and differentiation, Oxid. Med. Cell. Longev. (2015), 105135, https://doi.org/10.1155/2015/105135, 2015.
[38] Y.E. Henrotin, P. Bruckner, J.P.L. Pujol, The role of reactive oxygen species in homeostasis and degradation of cartilage, Osteoarthritis Cartilage 11 (2003) 747–755, https://doi.org/10.1016/s1063-4584(03)00150-x.
[39] C.R. Tim, C.C.S. Martignago, L. Assis, L.M. Neves, A.L. Andrade, N.C. Silva, N. Parizotto, K.Z. Pinto, A.C. Rennó, Effects of photobiomodulation therapy in chondrocyte response by in vitro experiments and experimental model of osteoarthritis in the knee of rats, Laser Med. Sci. 37 (2022) 1677–1686, https://doi.org/10.1007/s10103-021-03417-8.
[40] D.A. Zaky, R.H. Sayed, Y.S. Mohamed, Liraglutide limits the immunogenic cell death-mediated ROS propagation and PI3K/AKT inactivation after doxorubicin-induced gonadotoxicity in rats: involvement of the canonical Hedgehog trajectory, Int. Immunopharm. 119 (2023), 110212, https://doi.org/10.1016/j.intimp.2023.110212.
[41] M. Feng, D. Kong, H. Guo, C. Xing, J. Lv, H. Bian, N. Lv, C. Zhang, D. Chen, M. Liu, Y. Yu, L. Su, Gelsevirine improves age-related and surgically induced osteoarthritis in mice by reducing STING availability and local inflammation, Biochem. Pharmacol. 198 (2022), 114975, https://doi.org/10.1016/j.bcp.2022.114975.
[42] Y. Chen, Z. Zhang, Y. Xin, Z. Yu, X. Meng, Y. Zhang, D. He, Y. Zhang, Functional Transdermal Nanoethosomes enhance photodynamic therapy of hypertrophic scars via self-generating oxygen, ACS Appl. Mater. Interfaces 13 (2021) 7955–7965, https://doi.org/10.1021/acsami.0c20667.
[43] B.L. Yin, Y.P. Wang, C. Zhang, Y. Zhao, Y.J. Wang, L.L. Teng, Y. Yang, Z.B. Zeng, S. Y. Huan, G.S. Song, X.B. Zhang, Oxygen-embedded Quinoidal acene based semiconducting chromophore nanoprobe for amplified photoacoustic imaging and photothermal therapy, Anal. Chem. 91 (2019) 15275–15283, https://doi.org/10.1021/acs.analchem.9b04429.
[44] Y.D. Yang, T.X. Yang, F.F. Chen, C. Zhang, B.L. Yin, X. Yin, L.B. Han, Q.J. Xie, X. B. Zhang, G.S. Song, Degradable magnetic nanoplatform with Hydroxide ions triggered photoacoustic, MR imaging, and photothermal conversion for precise cancer Theranostic, Nano Lett. 22 (2022) 3228–3235, https://doi.org/10.1021/acs.nanolett.1c04804.